NASA TECHNICAL NOTE

NASA TN D-7696

NASA TN D-7696

FLIGHT-MEASURED INLET PRESSURE TRANSIENTS ACCOMPANYING ENGINE COMPRESSOR SURGES ON THE F-111A AIRPLANE

by Jack Nugent and Jon K. Holzman

Flight Research Center
Edwards, Calif. 93523

NATIONAL AERONAUTICS AND SPACE ADMINISTRATION • WASHINGTON, D. C. • JUNE 1974

1. Report No.	2. Government Accession No.	3. Recipient's Catalog No.
NASA TN D-7696		

4. Title and Subtitle	5. Report Date
FLIGHT-MEASURED INLET PRESSURE TRANSIENTS ACCOMPANYING ENGINE COMPRESSOR SURGES ON THE F-111A AIRPLANE	JUNE 1974
	6. Performing Organization Code

7. Author(s)	8. Performing Organization Report No.
Jack Nugent and Jon K. Holzman	H-804
	10. Work Unit No.
9. Performing Organization Name and Address	766-76-01
NASA Flight Research Center P. O. Box 273 Edwards, California 93523	11. Contract or Grant No.
	13. Type of Report and Period Covered
12. Sponsoring Agency Name and Address	Technical Note
National Aeronautics and Space Administration Washington, D. C. 20546	14. Sponsoring Agency Code

15. Supplementary Notes

16. Abstract

Two F-111A airplanes were subjected to conditions that caused engine compressor surges and accompanying duct hammershock pressure transients. Flight speed ranged from Mach 0.71 to Mach 2.23, and altitude varied from approximately 3200 meters (10,600 feet) to 14,500 meters (47,500 feet). A wide range of compressor pressure ratios was covered.

Stabilized free-stream, engine, and duct conditions were established before each compressor surge. Dynamic pressure instrumentation at the compressor face and in the duct recorded the pressure transients associated with the surges. Hammershock pressures were analyzed with respect to the stabilized conditions preceding the compressor surges.

The hammershock transients caused large pressure rises at the compressor face and in the duct. Hammershock pressure ratios at the compressor face were not affected by free-stream Mach number or altitude but were functions of engine variables, such as compressor pressure ratio. The maximum hammershock pressure ratio of approximately 1.83 occurred at a compressor pressure ratio of approximately 21.7.

Normalized hammershock pressures measured on the inboard wall of the duct increased linearly with duct Mach number preceding the compressor surge. Hammershock transit time through the duct was approximately 3 milliseconds per meter (1 millisecond per foot).

17. Key Words (Suggested by Author(s))	18. Distribution Statement
Nonsteady inlet flow Inlet engine compatibility Duct flow dynamics	Unclassified - Unlimited CAT. 28

19. Security Classif. (of this report)	20. Security Classif. (of this page)	21. No. of Pages	22. Price*
Unclassified	Unclassified	28	$4.25

FLIGHT-MEASURED INLET PRESSURE TRANSIENTS ACCOMPANYING ENGINE COMPRESSOR SURGES ON THE F-111A AIRPLANE

Jack Nugent and Jon K. Holzman
Flight Research Center

INTRODUCTION

In designing propulsion systems for advanced supersonic aircraft, it is becoming increasingly important to avoid adverse dynamic flow interactions between the inlet and the engine, particularly when a large flight envelope must be covered. One type of adverse flow interaction is caused by an engine compressor surge which generates a large transient pressure rise at the engine compressor face that propagates rapidly upstream through the duct. This transient pressure rise is known as a hammershock. Hammershocks were measured during ground tests on subscale and full-scale inlets in the studies of references 1 to 4. To supplement these data and provide a more useful basis for advanced supersonic aircraft design, the NASA Flight Research Center made a flight study of the inlet-engine flow interactions on two specially instrumented, supersonic F-111A airplanes (refs. 5 to 8). In these flight tests (ref. 7) numerous compressor surges were deliberately induced. Most of the data were obtained at the compressor face of the F-111A number 12 airplane. Additional data were obtained at the compressor face and through the duct of the F-111A number 6 airplane. Steady-state and dynamic propulsion system pressure phenomena, except the hammershocks that occurred during the tests, are analyzed in reference 7.

This report presents hammershock data obtained on both airplanes during 21 selected tests in which hammershocks resulted from engine compressor surges. During these tests, airspeed ranged from Mach 0.71 to Mach 2.23 and altitude varied from approximately 3200 meters (10,600 feet) to 14,500 meters (47,500 feet). These conditions cover most of the F-111A flight envelope. Data are also presented from a static ground test made at Edwards Air Force Base, Calif.

A wide range of compressor pressure ratios was covered during the flight tests. Absolute hammershock pressures and normalized hammershock pressure ratios at the compressor face of the number 12 airplane are analyzed with respect to the stabilized engine, duct, and free-stream flow conditions immediately before the compressor surge. Hammershock pressures in the duct and hammershock propagation upstream through the duct of the number 6 airplane are also analyzed.

SYMBOLS

Physical quantities in this report are given in the International System of Units (SI) and parenthetically in U.S. Customary Units. The measurements were taken in U.S. Customary Units. Factors relating the two systems are presented in reference 9.

A	duct cross-sectional area, m^2 (ft^2)
h_p	altitude, m (ft)
M	Mach number
N_1	low-pressure compressor rotor speed, rpm
p	static pressure, kN/m^2 (lbf/in^2)
Δp	duct hammershock pressure, kN/m^2 (lbf/in^2) (see fig. 9)
p_t	total pressure, kN/m^2 (lbf/in^2)
T_t	total temperature, °K (°R)
t	time, sec
Δt	time for the hammershock to travel from the compressor face to a duct station, msec (see fig. 9)
V	velocity, m/sec (ft/sec)
w	airflow, kg/sec (lbm/sec)
X/R	ratio of distance between inlet cowl lip and spike tip, X, to inlet cowl radius, R (R = 84.56 cm (33.29 in.))
δ	ratio of inlet total pressure to standard-day sea-level static pressure
θ	ratio of total temperature to standard-day sea-level temperature
θ_c	second cone angle, deg

Subscripts:

A,B,C,D	instrumentation stations in the duct (see fig. 5)
b	peak of the hammershock pressure pulse
c	cowl

core	core section of engine
s	average net hammershock speed from compressor face to cowl lip
2	compressor face station
4	compressor exit station
∞	free stream

A prime denotes a stabilized condition immediately before a compressor surge and hammershock.

AIRPLANE AND PROPULSION SYSTEM

The F-111A airplane (fig. 1) is a multimission, variable-wing-sweep fighter airplane that can fly at speeds greater than Mach 2. With the wings swept forward, it is capable of short takeoffs and landings and efficient subsonic flight. With the wings swept back, it can fly supersonically at high and low altitudes. The two airplanes used in this study, number 6 (S/N 639771) and number 12 (S/N 639777), were early models and not entirely representative of production models.

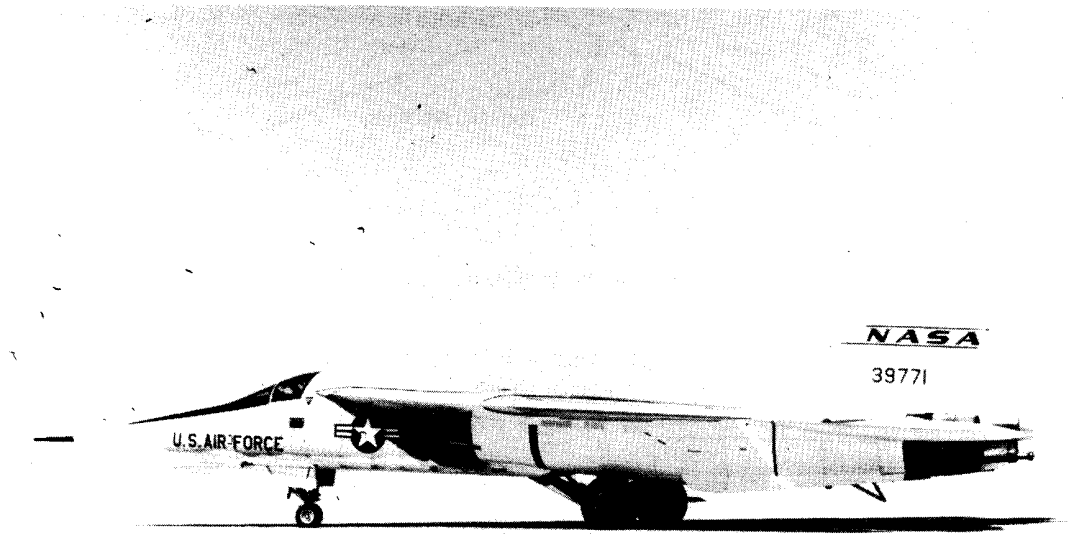

E-20270

Figure 1. F-111A airplane.

A drawing of the left half of the twin F-111A propulsion system is shown in figure 2. The system consists of an external compression inlet under the wing in the wing root area followed by a relatively short subsonic diffuser. The duct feeds air to a Pratt & Whitney TF30-P-1 afterburning turbofan engine which has a blow-in-door ejector nozzle integrated into the rear fuselage section. The inlet incorporates a variable-geometry, one-quarter, axisymmetric double cone for supersonic compression. The compression surface translates forward and rearward a maximum of 46 centimeters (18 inches) on the number 6 airplane and 50 centimeters (19.6 inches) on the number 12 airplane. The first cone has a fixed 12.5° half angle, and the second cone is variable from 10.5° to 24°. (Hereafter in this paper the first cone is referred to as the spike and the second cone as the cone.)

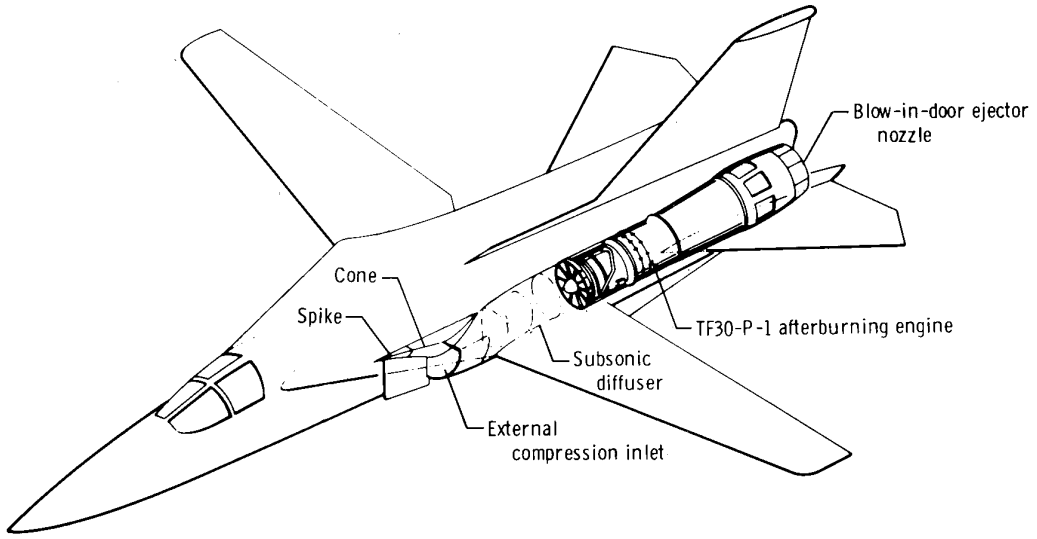

Figure 2. F-111A propulsion system. Left half.

As the airplane accelerates from Mach 1.1 to maximum speed, the spike and cone travel from a full-forward position to a full-rearward position. Concurrently, the cone moves from a fully collapsed to a fully expanded position. Detailed operational schedules are included in reference 7. These inlet geometry changes are controlled to scheduled settings by the automatic inlet control system which senses engine airflow and inlet local Mach number. In addition, the left inlet geometry of both airplanes was manually controllable by the pilot to off-schedule settings required for some test conditions.

The variable positions of the spike and cone result in changes in the inlet entrance area at the cowl lip as well as in the area progression in the forward portion of the duct. The data for the number 6 airplane were obtained with a sharp-lip and a blunt-lip cowl. The area distribution for these two test configurations is shown in figure 3. The data for the number 12 airplane were obtained with a sharp-lip cowl only. Reference 5 presents additional information on the cowl configuration.

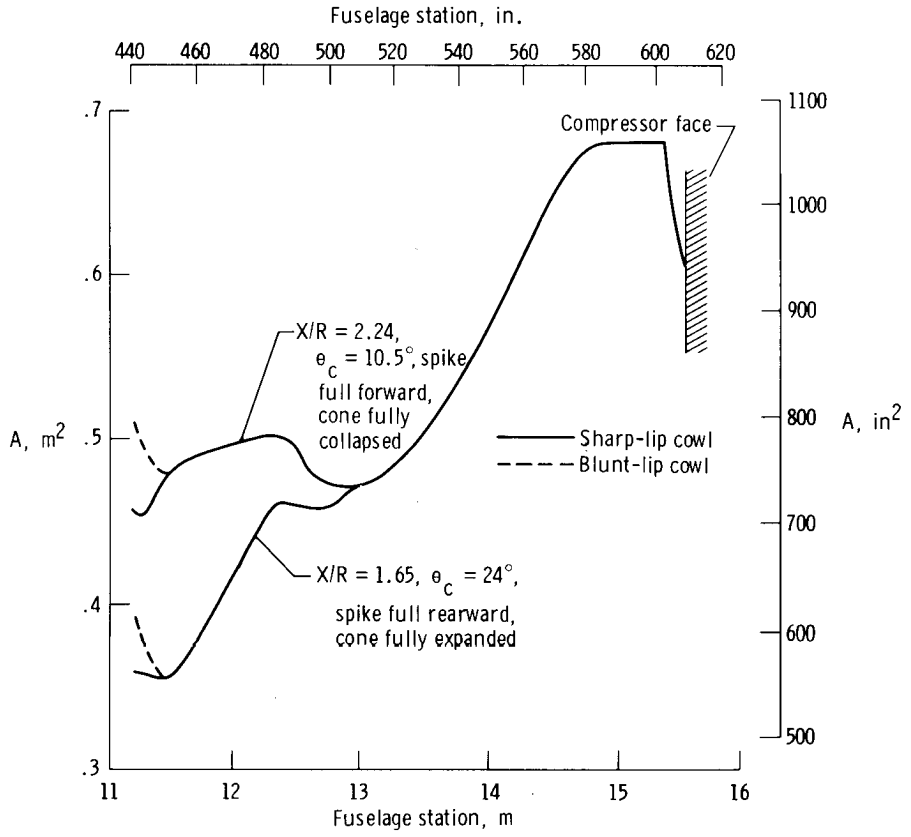

Figure 3. Duct area distribution on number 6 airplane.

The TF30-P-1 afterburning turbofan engine was rated in the 80-kilonewton (18,000-pound force) static-thrust class at sea level in full afterburning power. Rated airflow was 108 kg/sec (235 lbm/sec) at a nominal bypass ratio of approximately 0.9. The three-stage fan was integral with the six-stage low-pressure compressor; both were driven by a three-stage turbine. The seven-stage high-pressure compressor was driven by a single-stage turbine. The engines in both airplanes had been "rematched" to modify compressor stage loading and hence increase the stall margin. Stall margin was also increased by an automatic twelfth-stage bleed and a manually operated sixth-stage bleed.

Additional details on the airplane and propulsion system are included in references 5 to 7.

INSTRUMENTATION

Both test airplanes were instrumented to obtain in-flight measurements of free-stream and propulsion system parameters. Test data were recorded on board the airplanes with a tape recorder and telemetered to a ground receiving station. The free-stream parameters pertinent to this study were Mach number, altitude, and total

pressure. Instrumentation on the left propulsion system was positioned at the compressor face, through the duct, and on the cone. This instrumentation is discussed in the following sections and in references 5 to 8 and 10.

Compressor Face

Number 12 airplane.—Forty compressor face total pressures were sensed on the number 12 airplane by eight high-response rakes spaced radially at 45° angles (fig. 4). Each rake was self-nulling and had five pitot tubes positioned at the centers of equal annular areas. Miniature differential-pressure transducers were mounted internally in the rake body behind each probe to minimize pneumatic attenuation. The close coupling provided a frequency-response output flat to approximately 400 hertz, as reported in reference 5. In addition each rake had a unique nulling valve which permitted zero shifts caused by changing environmental conditions, especially temperature, to be measured and subsequently corrected for (ref. 8). This correction made it possible to accurately determine stabilized pressures before a surge occurred. Each differential-pressure transducer was connected to a reference absolute-pressure transducer so that absolute pressures could be obtained at the compressor face.

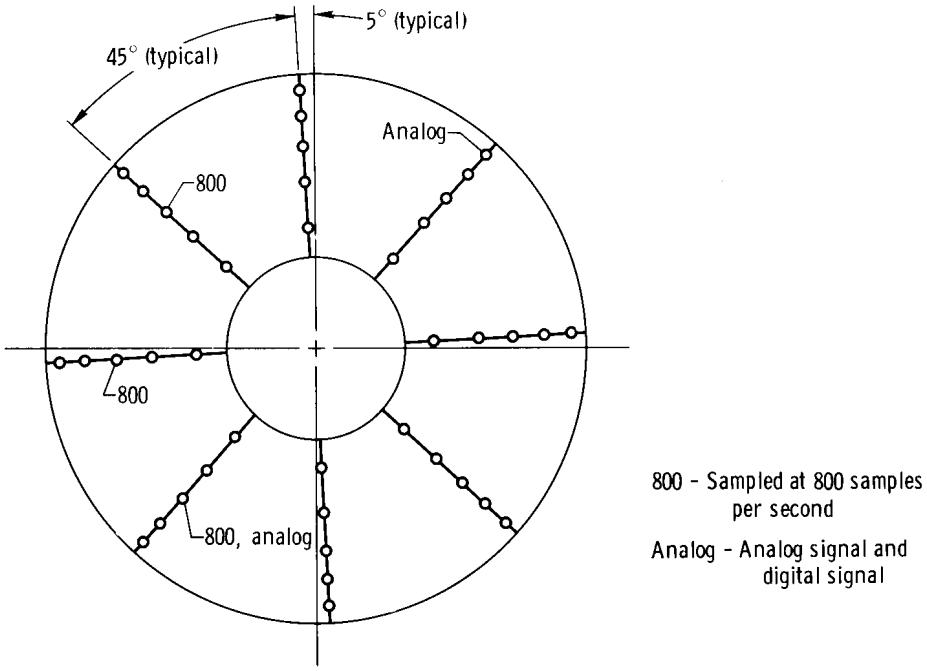

Figure 4. Compressor face total-pressure rake instrumentation on number 12 airplane. Left engine, looking rearward.

Number 6 airplane.—Eight compressor face total-pressure rakes (figs. 5(a) and 5(b)) were installed on the number 6 airplane in a manner similar to that used on the number 12 airplane. The diagonally oriented rakes at 1: 30, 4: 30, 7: 30, and 10: 30 o'clock were designed for high response and were like the compressor face rakes on the number 12 airplane, except that they did not have nulling capability.

These rakes were used in the hammershock analysis. The rakes at the 12: 00, 3: 00, 6: 00, and 9: 00 o'clock positions were not designed for high response.

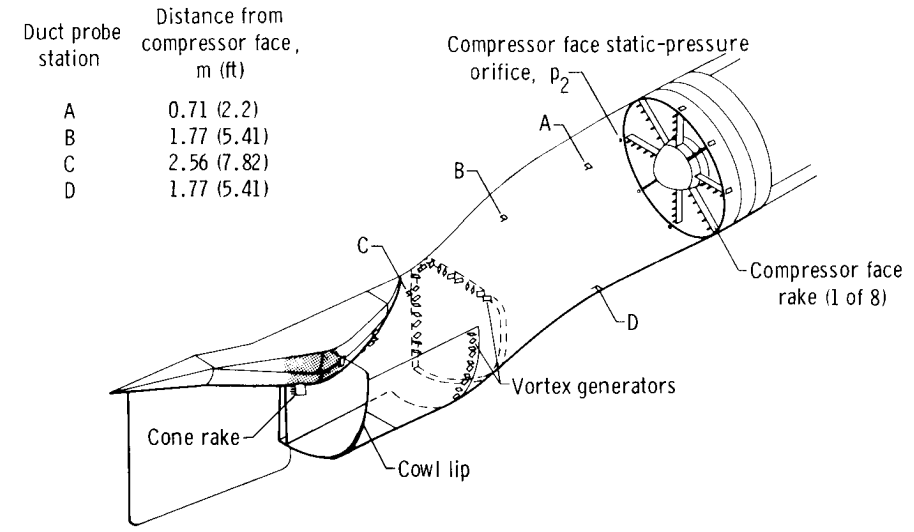

(a) Duct instrumentation.

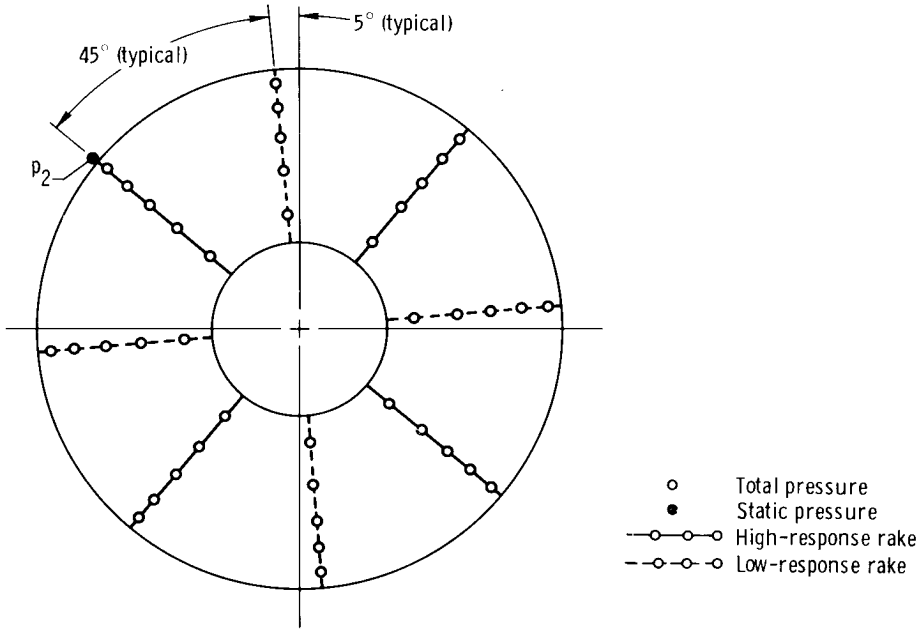

(b) Compressor face instrumentation, looking rearward.

Figure 5. Duct and compressor face pressure instrumentation on number 6 airplane.

Static pressure at the compressor face was measured by using a flush orifice installed in the duct wall at the 10: 30 o'clock rake. This static-pressure installation utilized a close-coupled miniature pressure transducer which had a frequency response that was flat to approximately 100 hertz.

Duct and Cone

The duct instrumentation shown in figure 5(a) for the number 6 airplane was used to measure pressures upstream of the compressor face and the transit time of the propagating hammershock. Pitot and static pressures were measured by probes at four stations (A,B,C,D) between the cone and the compressor face. Static pressure was also measured at the base of a rake on the cone surface. All the upstream measuring stations had close-coupled miniature pressure transducers which provided a frequency response above 200 hertz.

DATA ACQUISITION

Data were sampled and digitized during flight with an onboard pulse code modulation (PCM) system that could handle 77 data channels at 200 samples per second. To avoid aliasing errors in the analysis, each channel was filtered before it was digitized. For the high-response data channels, an active three-pole, low-pass Butterworth filter was used to provide linear filtering out to the cutoff frequency of 200 hertz with sharp attenuation (rolloff) characteristics of 18 decibels per octave beyond 200 hertz.

Number 12 Airplane

The 40 pitot pressures measured on the number 12 airplane were supercommutated to provide 400-sample-per-second data, twice the basic commutation rate, to increase frequency response. In addition three of the 40 pressures were further supercommutated to provide 800-sample-per-second data (fig. 4) to improve the analysis of transients, such as hammershocks.

In addition to the PCM system, two high-response total pressures on opposite sides of the compressor face were simultaneously recorded on wide-band frequency-modulated analog channels. One of these pressures was one of the three that were digitized at 800 samples per second. A direct comparison between analog and digital data was made for selected hammershock transients. The results showed no degradation of the 800-sample-per-second data compared to the analog data in determining the hammershock pressures, but some degradation of the 400-sample-per-second data. Therefore the 800-sample-per-second data were used to establish peak hammershock pressures.

Number 6 Airplane

The 20 high-response compressor face total pressures and the static pressure measured on the number 6 airplane were filtered at 200 hertz and sampled at

400 samples per second. The four duct total pressures and three of the duct static pressures were filtered at 40 hertz and digitized at 200 samples per second. The remaining duct static pressure and the cone surface pressure were filtered at 200 hertz and digitized at 400 samples per second.

TESTS

The airplanes were flown at Mach numbers from 0.71 to 2.23 and at altitudes from approximately 3200 meters (10,600 feet) to approximately 14,500 meters (47,500 feet) within the test envelope shown in figure 6. Data were obtained primarily from 21 tests on five research flights during which engine surges were encountered. Data were also obtained from a static ground test.

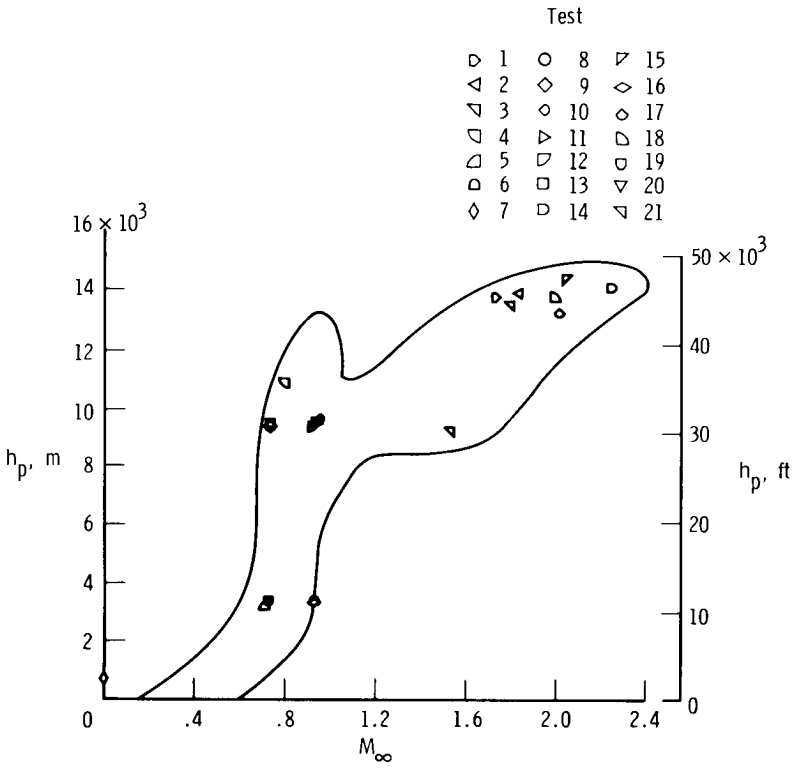

Figure 6. F-111A test envelope showing where engine compressor surges occurred.

Pressure data were obtained for a period starting just before an engine surge and ending slightly after the surge. Engine surges were induced by increasing the airplane angle of attack during a wind-up-turn maneuver or by manually varying the

inlet geometry to off-design values of spike or cone position. The airplanes were kept at stabilized flight conditions, and the engine power was not changed before the surge. After the surge the pilot usually discontinued the test and started engine recovery procedures.

ACCURACY

The accuracy of several measured and calculated parameters obtained from flight data for the number 6 airplane is presented in reference 5. The parameter accuracy for data from the number 12 airplane was similar except for the values of $(p_t)_2$. The use of nullable rakes and associated correction techniques made it possible to determine $(p_t)_2$ to approximately ±1 percent, as reported in reference 7. The following table lists the accuracy of parameters pertinent to this study. (Several of the accuracies presented in reference 5 are repeated.)

	Error
Number 6 airplane —	
M_∞	±0.005 at h_p = 3050 m (10,000 ft) ±0.008 at h_p = 9150 m (30,000 ft) and 13,700 m (45,000 ft)
h_p	±33.5 m (±110 ft)
$(p_t)_\infty$	±0.83 kN/m² (±0.12 lbf/in²)
T_t	±2.8° K (±5° R)
X/R	±1.0 percent
θ_c	±0.5°
$N_1/\sqrt{\theta}$	±1.4 percent
$\frac{w\sqrt{\theta}}{\delta}$	±2.0 percent
p_2	±1.2 percent
M_2'	±2.0 percent
$\Delta p_{duct}/(p_t)_\infty$	±2.6 percent
Number 12 airplane —	
M_2'	±2.0 percent
p_2'	±1.9 percent
p_4'	±2.5 percent
Bypass ratio	±10.0 percent
$(p_t)_2$	±1.1 percent
$(p_t)_b - p_2'$	±3.0 percent
$(p_t)_b/p_2'$	±3.0 percent

For the number 6 airplane, only incremental duct hammershock pressures, for example, $\Delta p_{duct}/(p_t)_\infty$, are presented. The absolute pressures were not considered reliable because of the transducer zero shifts caused by temperature changes.

DATA ANALYSIS

Theory

Hammershock strength.—Hammershock strength can be analyzed theoretically by assuming that one-dimensional steady flow in a constant-area-stream tube or duct is instantly reduced (refs. 11 and 12). Thus hammershock strength, as indicated by the transient duct pressures immediately following the flow reduction, can be related to the Mach number of the flow preceding the reduction and the amount of flow that is reduced. Duct pressures rise abruptly at the flow reduction station as a result of the formation of a normal shock wave or hammershock wave which travels rapidly upstream in the duct with undiminished strength. As the normal shock travels upstream, the walls of the duct behind the hammershock are exposed to the rise in pressure. For a flow reduction of 100 percent at the reduction station, all the duct flow is stopped instantly and is stagnated. For a flow reduction of less than 100 percent, only a portion of the flow is stopped instantly, and the remaining flow continues at a much lower Mach number. For a flow reduction of greater than 100 percent, all the duct flow is stopped instantly, and a portion of the flow is instantly reversed. For example, for a flow reduction of 200 percent, all the duct flow is reversed.

Figure 7 shows the results of a theoretical analysis of hammershock strength in a constant-area duct. In figure 7(a) the hammershock total pressure, $(p_t)_b$, is divided

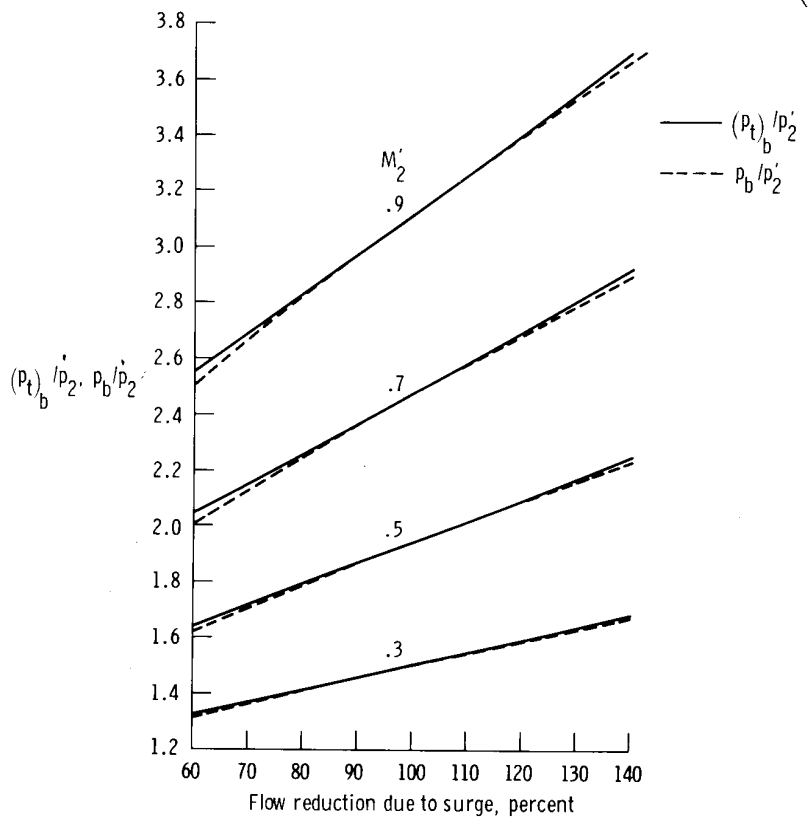

(a) Hammershock pressure ratios as a function of duct Mach number and flow reduction.

Figure 7. Hammershock theory for a constant-area duct.

by the steady-state static pressure, p_2, at the flow reduction station before the flow is reduced. This ratio and the hammershock static pressure ratio, p_b/p_2, are plotted against percent flow reduction for several duct Mach numbers. The data indicate that hammershock pressure ratios increase steadily with flow reduction for a given duct Mach number, and if the flow reduction is constant, the ratios increase with duct Mach number. At 100-percent flow reduction, the total- and static-pressure ratios are equal because the flow is stagnated. For flow reductions somewhat greater or less than 100 percent, the static-pressure ratio is only slightly less than the total-pressure ratio regardless of the flow direction, because the Mach number following the flow reduction, either upstream or downstream, is on the order of 0.1 or less. Thus, for practical purposes, the total and static hammershock pressures can be considered equal for the flow reduction range shown.

Hammershock propagation.—Hammershock theory also predicts the net speed of the hammershock traveling upstream in the constant-area duct as a function of duct Mach number and flow reduction. Predictions based on this theory are shown in figure 7(b). Net hammershock Mach number increases almost linearly with increasing flow reduction at a given duct Mach number, and if the flow reduction is constant, the net hammershock Mach number decreases with increasing duct Mach number.

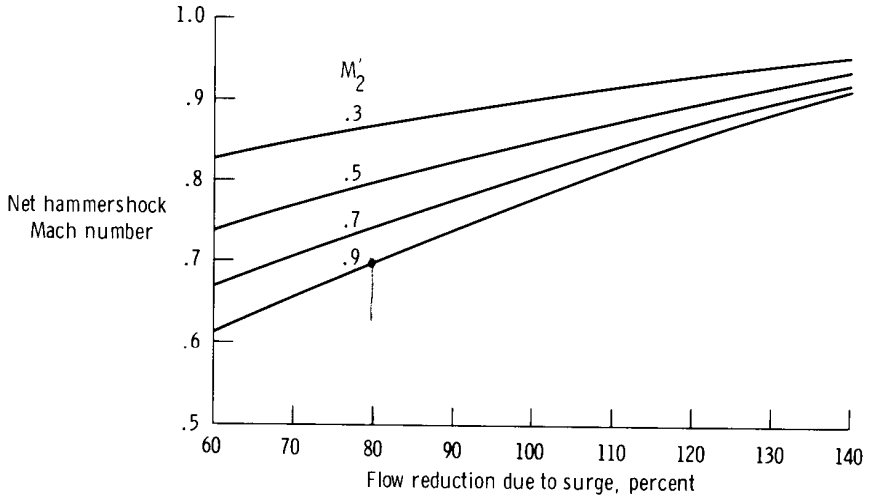

(b) Net hammershock Mach number as a function of duct Mach number and flow reduction.

Figure 7. Concluded.

Application of Theory to Flight Data

Hammershock strength.—Hammershock strength was determined from time histories of individual pressure traces such as those in figures 8 and 9. Hammershock pressures are indicated by point b in figures 8(a) to 8(e). For the compressor face these values were obtained from the three compressor face pitot probe pressures of the number 12 airplane sampled at 800 samples per second. These three pressures

were averaged to yield an overall hammershock pressure for the particular test. This hammershock pressure was taken as the hammershock strength at the compressor face.

Because duct Mach number and the amount of flow reduction govern theoretical hammershock strength, they were used to analyze the hammershock pressures. Duct Mach number at the compressor face increases steadily with corrected low rotor speed, $N_1/\sqrt{\theta}$, corrected airflow, $\frac{w\sqrt{\theta}}{\delta}$, and compressor pressure ratio, p_4'/p_2'; therefore, these parameters were also used to analyze the data. The effect of core airflow reduction on hammershock strength was determined by plotting hammershock pressure against core airflow before surge. Hammershock pressures were also compared with free-stream total pressure.

Hammershock propagation.—Duct hammershock pressures, Δp, for the number 6 airplane were obtained as shown in figure 9. As indicated, the transit time, Δt, of the hammershock was established by noting the time intervals associated with the start of the transient at the several duct stations. Transit time of the hammershock traveling through the fixed-geometry portion of the duct was compared with theory.

RESULTS AND DISCUSSION

Time Histories of Pressure Transients

Compressor face.—Figures 8(a) to 8(e) are time histories of selected compressor face pitot probe differential pressures obtained from the two test airplanes. The figures present data for a short time before the hammershock pulse, the pulse, and a period after the pulse. These time histories show that large pressure rises of various strengths were measured and that hammershock transient behavior after a pulse is not always the same. For example, in figure 8(a) point a designates the start of the pulse and point b the hammershock pressure (approximately 24 kN/m^2 (3.5 lbf/in^2)). The pressure remains high in the interval from point b to point c. In the interval from point a to c, the hammershock propagates through the duct, reaches the cowl lip, and is expelled. Thus, the hammershock overpressurizes the entire duct. From point c to point d the pressure decays when the high-pressure air in the duct leaves through the cowl entrance. This pressure decay is analyzed in reference 10. Recovery associated with the resumption of airflow downstream through the duct starts at point d. At point e conditions become similar to those at point a, indicating complete recovery from the transient.

Figure 8(b) shows another kind of transient behavior following a hammershock pulse. The conditions at points a, b, c, and d are similar to those at the corresponding points in figure 8(a); however, complete recovery from the hammershock transient to the original conditions of point a does not occur. Instead, at point e a rotating stall starts at an average pressure level significantly higher than the pressure at point a.

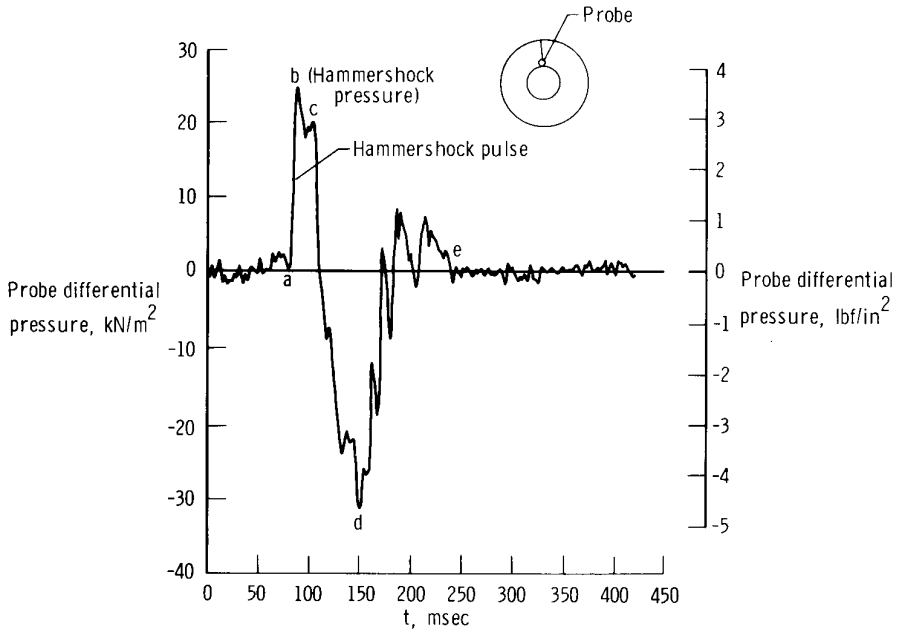

(a) Hammershock transient followed by recovery. Test 3.

Figure 8. Time histories of selected compressor face probe differential pressures obtained from both airplanes. 400-sample-per-second data.

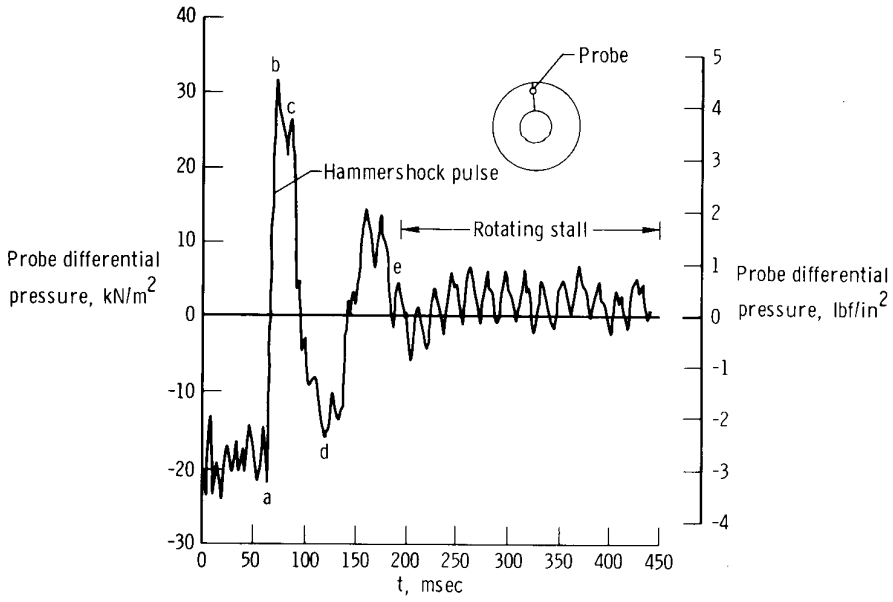

(b) Hammershock transient followed by a rotating stall. Test 6.

Figure 8. Continued.

Figure 8(c) shows data for a hammershock pulse that was preceded and followed by a rotating stall. The rotating stall continued after the recovery from the hammershock pulse. Reference 7 analyzes the effects of a rotating stall on compressor face pressures before and after a hammershock pulse.

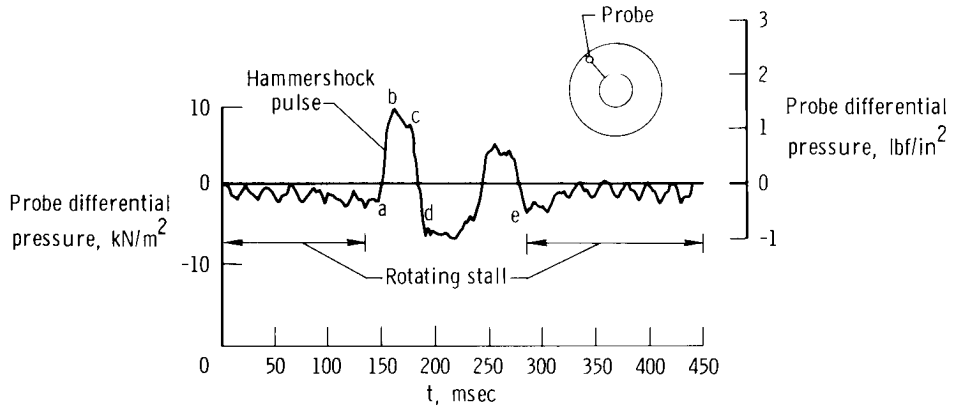

(c) Hammershock transient preceded and followed by a rotating stall. Test 13.

Figure 8. Continued.

Figures 8(d) and 8(e) illustrate two additional kinds of transient behavior that can follow a hammershock pulse. In figure 8(d) an apparent recovery is indicated at point e after the first hammershock pulse. However, the distortion that caused the first engine surge persisted and a second surge and hammershock occurred. Figure 8(e) illustrates several buzz cycles which were induced by a hammershock pulse. The buzz cycles are associated with cyclic motion of the inlet shock system. F-111 buzz amplitudes and frequencies, such as shown in figure 8(e), are analyzed in reference 7.

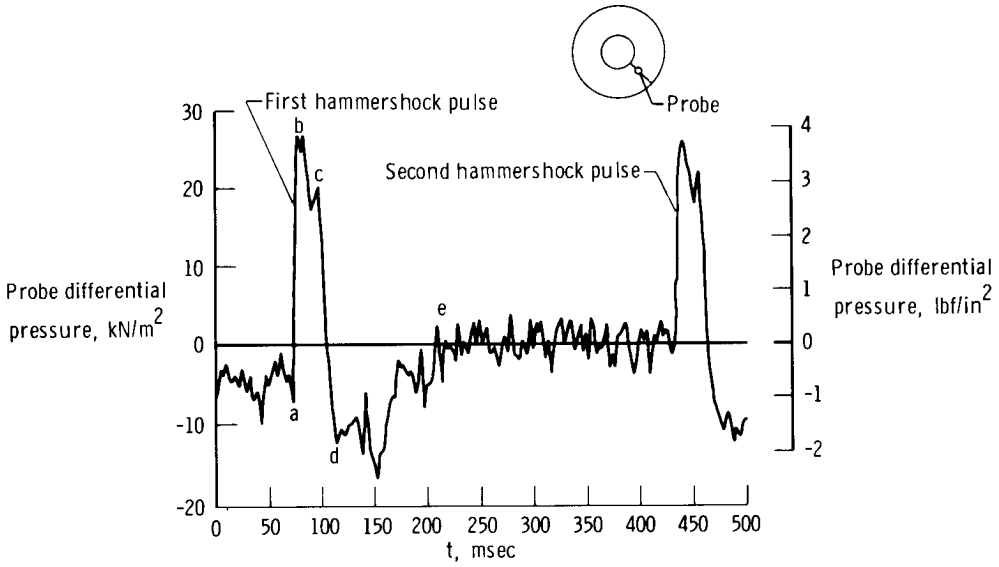

(d) Two hammershock transients. Test 5.

Figure 8. Continued.

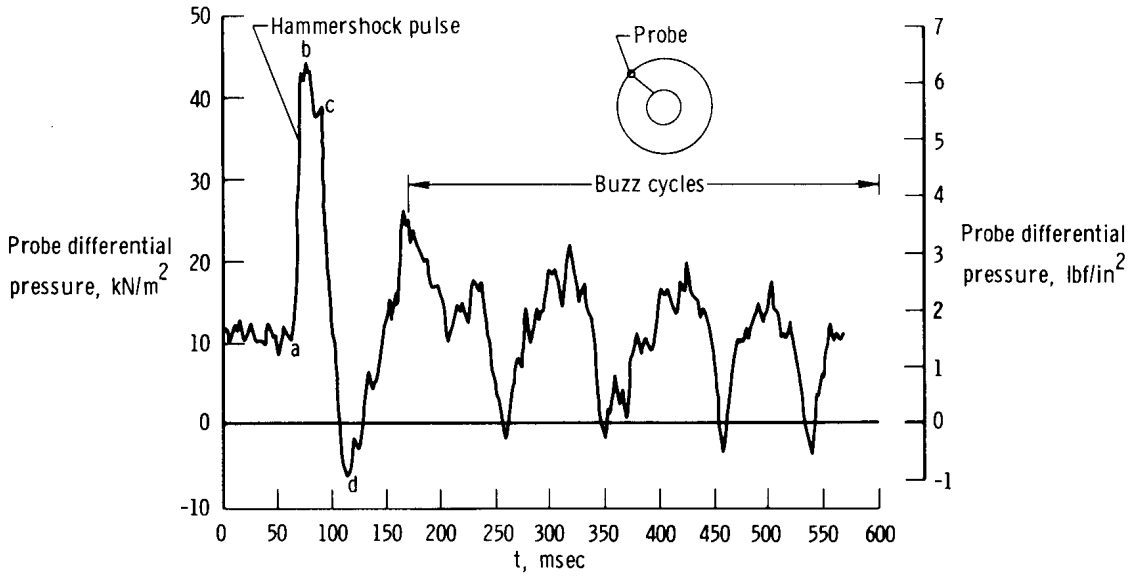

(e) Hammershock transient followed by buzz cycles. Unlisted test.

Figure 8. Concluded.

Hammershock propagation.—Figure 9 is a partial time history of the three inboard duct wall pressures and pressures on the compressor face and cone surface during a hammershock in the number 6 airplane (stations A, B, and C). The hammershock transit time, Δt, increased steadily from zero at the compressor face to 9 milliseconds after it passed through stations A, B, and C. The pressure pulse on the cone surface shows that the hammershock effects extended upstream of the cowl lip.

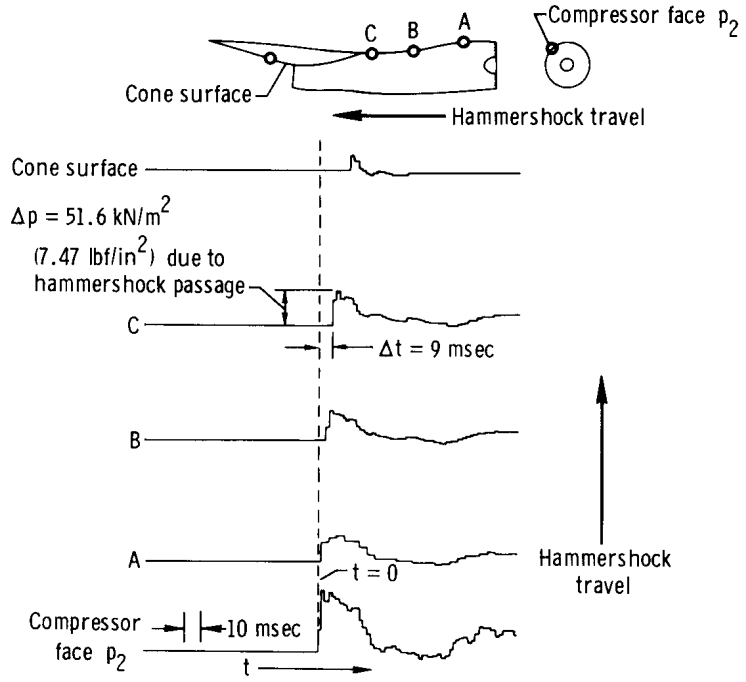

Figure 9. Partial time history of duct pressures resulting from surge on test 21 showing how pressures and transit times were obtained.

Compressor Face Hammershock Pressures

The data used to analyze compressor face hammershock pressures of the number 12 airplane are shown in table 1. The parameter w_{core} was obtained by dividing the absolute airflow through the duct by 1 + bypass ratio. The bypass ratio was obtained from the engine manufacturer's estimates and was a function of $\frac{w\sqrt{\theta}}{\delta}$.

Figure 10 shows the engine cycle parameters p'_4/p'_2, $\frac{w\sqrt{\theta}}{\delta}$, and $N_1/\sqrt{\theta}$ and the hammershock pressure ratios $(p_t)_b/p'_2$ and $(p_t)_b/p'_4$ as a function of duct Mach number. The parameters p'_4/p'_2, $\frac{w\sqrt{\theta}}{\delta}$, and $N_1/\sqrt{\theta}$ (fig. 10(a)) show the

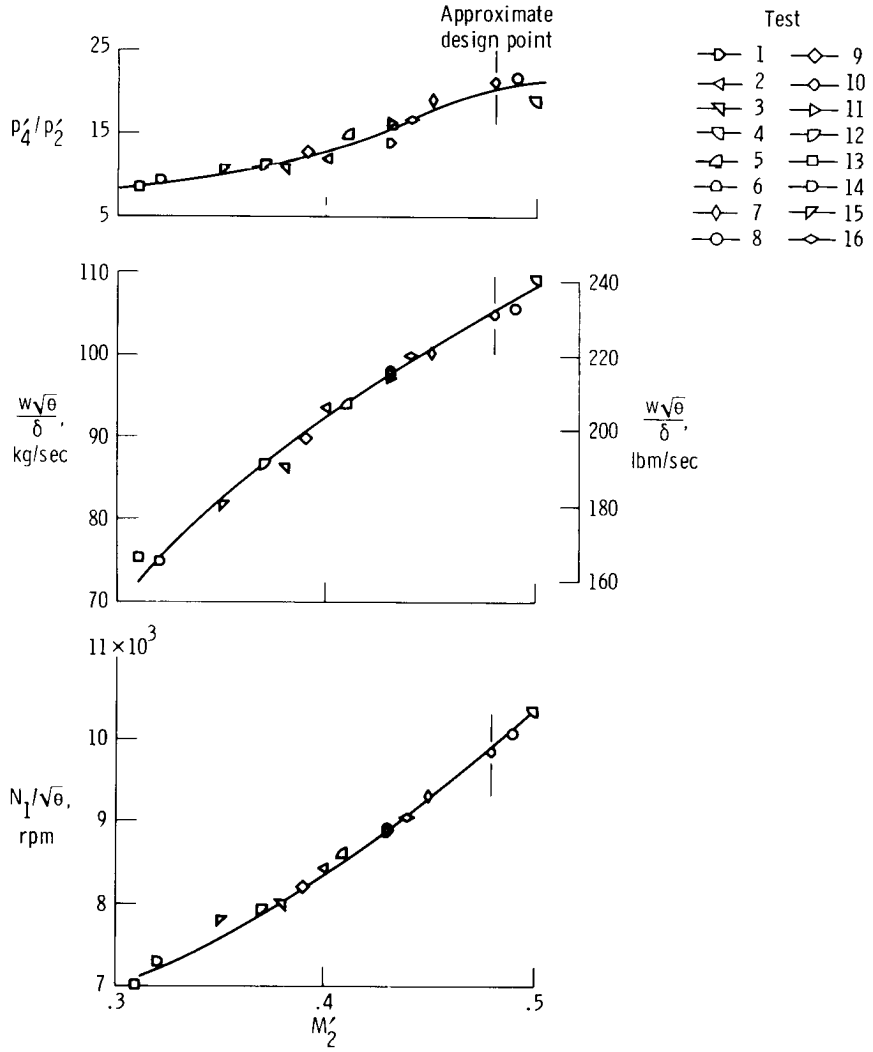

(a) Engine flow variables measured before surge.

Figure 10. Variation of engine flow variables and hammershock pressure ratios with M'_2.

characteristic steady-state relationships for a compressor or fan, that is, a steady increase as M'_2 increases. Maximum test values of M'_2 and p'_4/p'_2 exceeded the engine manufacturer's approximate sea-level static standard-day design points. Similarly, the hammershock pressure ratios $(p_t)_b/p'_2$ and $(p_t)_b/p'_4$ (fig. 10(b)) generalize into reasonably well-defined curves when plotted against M'_2. The parameter $(p_t)_b/p'_2$ increases with increasing M'_2, whereas $(p_t)_b/p'_4$ decreases with increasing M'_2. The peak value of $(p_t)_b/p'_2$ occurs close to the approximate M'_2 design point, and the minimum value of $(p_t)_b/p'_4$ is near the approximate M'_2 design point. Theoretical predictions of $(p_t)_b/p'_2$ corresponding to 100-percent and 80-percent duct flow reductions at the compressor face are also shown in the figure. On the basis of these theoretical results, the flight data may be interpreted as showing an increasing flow reduction as M'_2 increases, possibly because of the decrease of bypass ratio with increasing M'_2 shown in table 1. The flow reduction near the design point is approximately 90 percent.

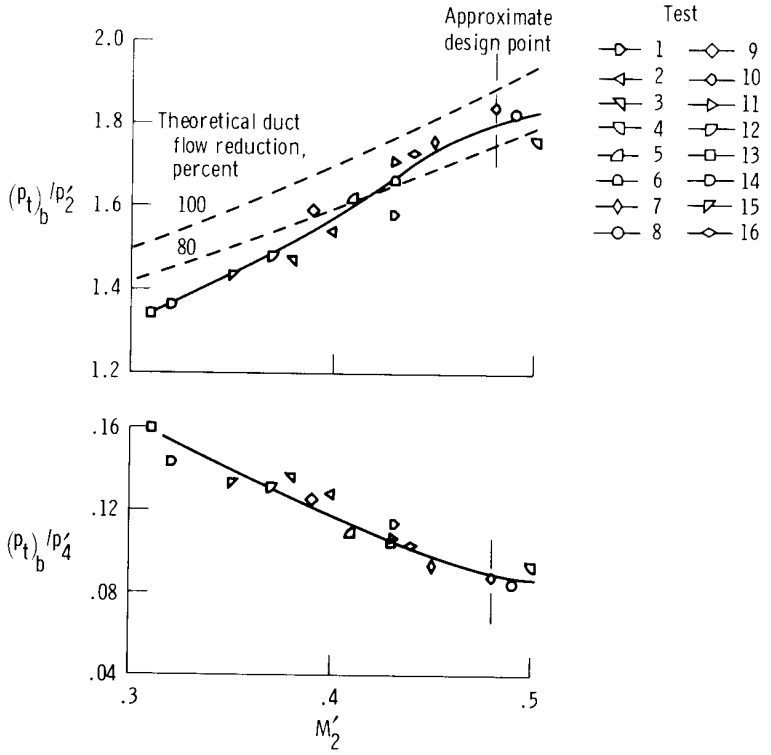

(b) Hammershock pressure ratios.

Figure 10. Concluded.

Figure 10 shows that engine cycle parameters, as well as M'_2, can be used to determine compressor face hammershock pressure ratios. In figure 11 hammershock pressure ratios $(p_t)_b/p'_2$ and $(p_t)_b/p'_4$ are plotted against compressor static-pressure ratio. The data in figure 11(a) show a well-defined curve that increases from $(p_t)_b/p'_2 \approx 1.3$ at $p'_4/p'_2 \approx 8.4$ to $(p_t)_b/p'_2 \approx 1.85$ at $p'_4/p'_2 \approx 22$. The test limit for p'_4/p'_2 of approximately 22 exceeds the approximate design point of 19.3. The peak value of $(p_t)_b/p'_2$ of approximately 1.85 is at the test limit of p'_4/p'_2. Figure 11(b) also shows a well-defined curve which decreases from $(p_t)_b/p'_4 \approx 0.16$ at $p'_4/p'_2 \approx 8.4$ to $(p_t)_b/p'_4 \approx 0.08$ at $p'_4/p'_2 \approx 22$. Reference 13, which analyzes hammershock pressures for several engines in a manner similar to that of figure 11, also shows that hammershock pressure ratio increases with compressor pressure ratio.

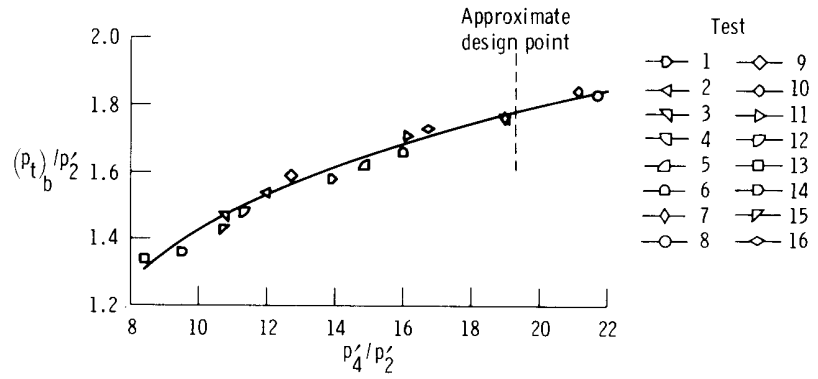

(a) $(p_t)_b/p'_2$.

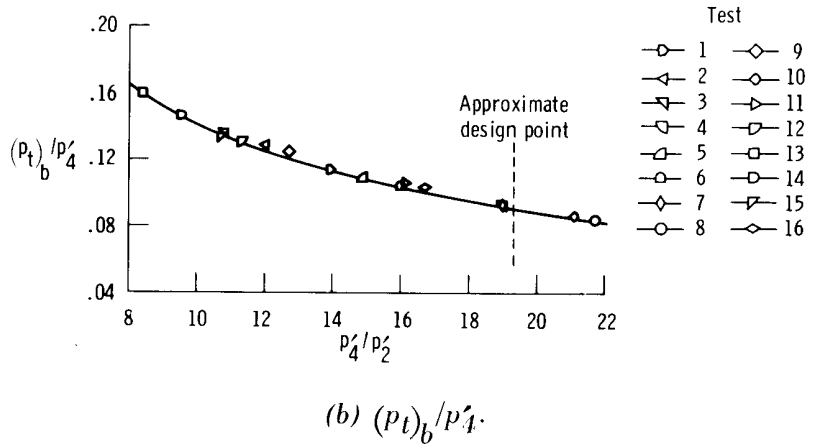

(b) $(p_t)_b/p'_4$.

Figure 11. Effect of compressor static-pressure ratio on hammershock pressure ratios $(p_t)_b/p'_2$ *and* $(p_t)_b/p'_4$.

The data of reference 14 indicate that surges start in the core portion of the TF30 engine. Therefore, because approximately 100 percent of the core flow is stopped during surge, a plot of hammershock pressure rise against core flow yields the linear relationship shown in figure 12.

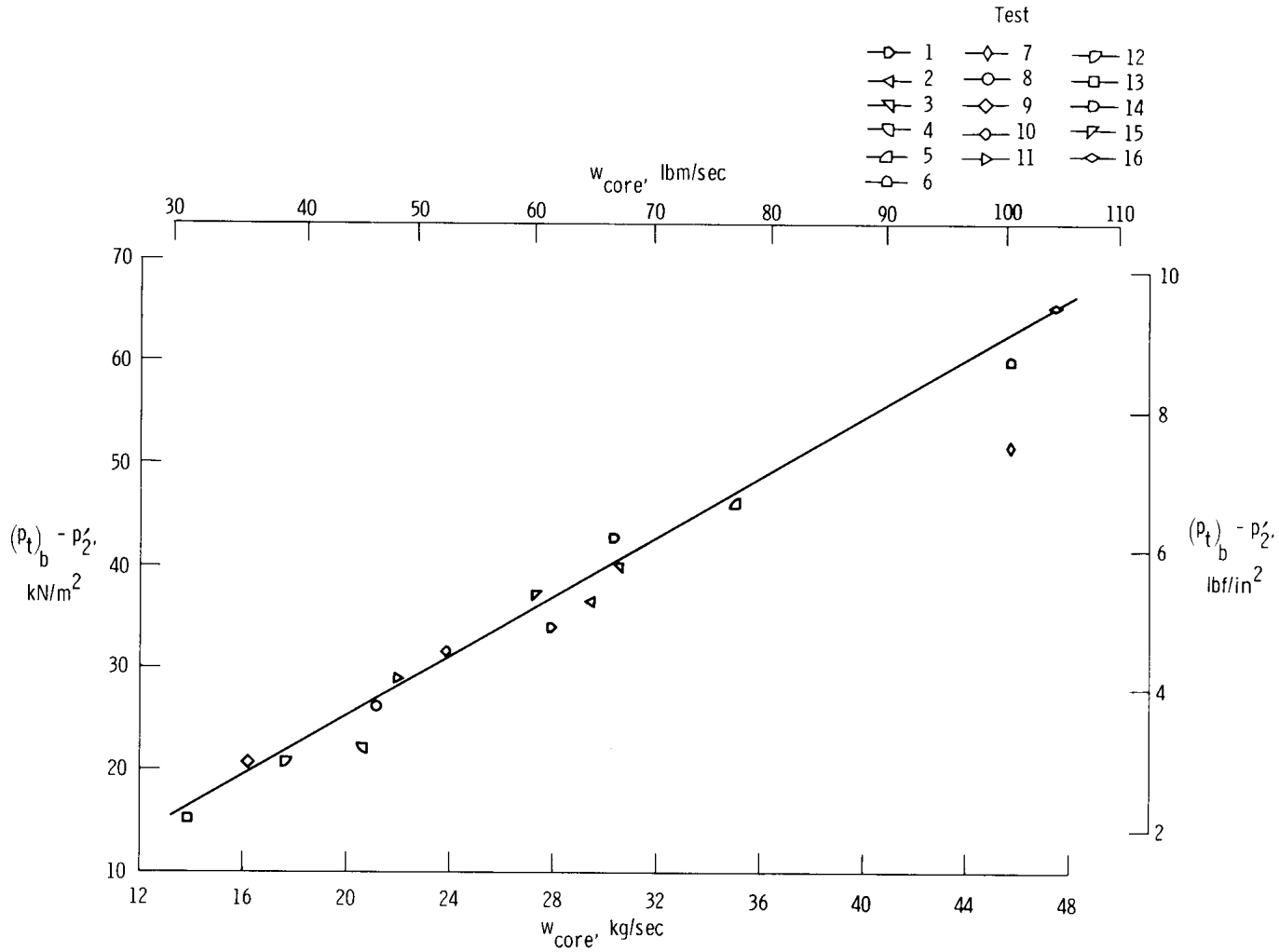

Figure 12. Variation of hammershock pressure rise with core airflow.

The data trends of figures 10 to 12 and the data in table 1 show no discernible effects of free-stream Mach number or altitude on hammershock pressures. Therefore, hammershock pressures measured at the compressor face during the tests are considered to be independent of these variables.

Compressor face hammershock pressure is plotted against free-stream total pressure, $(p_t)_\infty$, in figure 13. In every test, hammershock pressure exceeded the free-stream total pressure; most of the data show increases of 14 kN/m^2 to 28 kN/m^2 (2 lbf/in^2 to 4 lbf/in^2) over values of $(p_t)_\infty$. On two tests the increase was approximately 35 kN/m^2 (5 lbf/in^2), as shown.

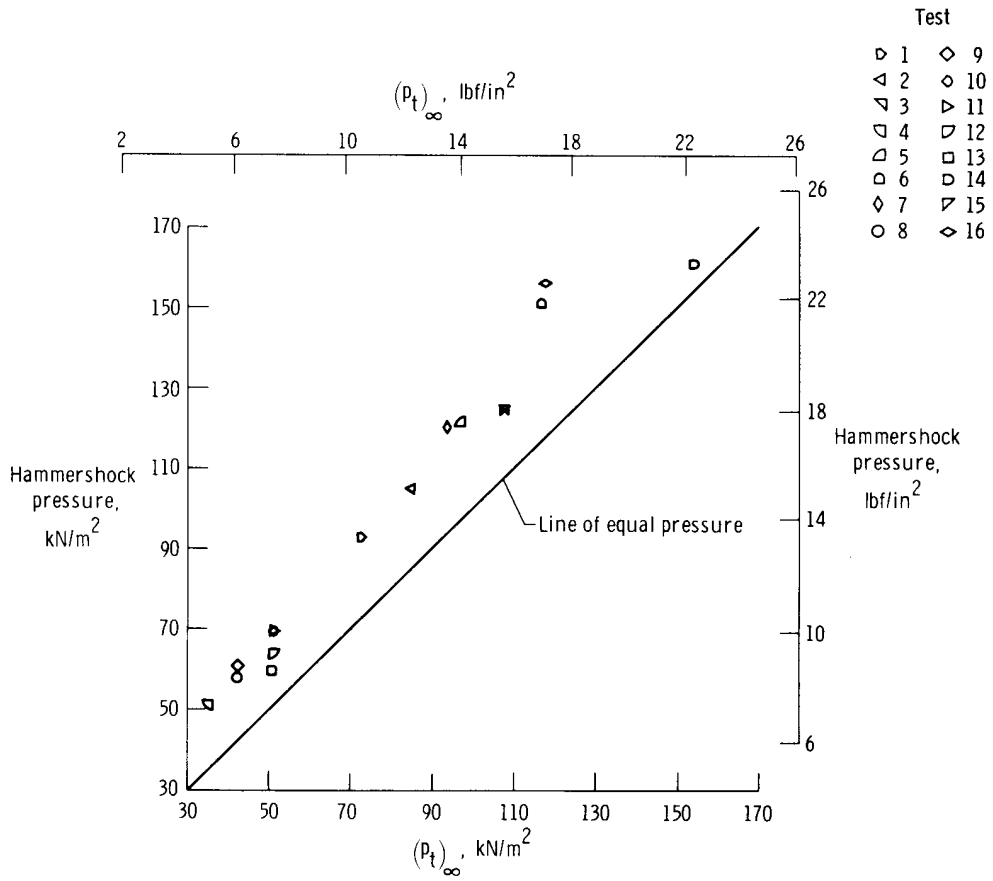

Figure 13. Hammershock pressure as a function of free-stream total pressure.

Hammershock Propagation

The parameters used to analyze hammershock propagation through the duct of the number 6 airplane are shown in table 2. The pressure rises on the inlet cone indicate that the hammershock was expelled ahead of the cowl lip for these tests. The inlet cone pressure rises are less than pressure rises measured in the duct. These results suggest that the hammershock strength decreases after the hammershock leaves the duct, but does not decrease to zero. Therefore, hammershock transient pressures can affect nearby portions of the airplane ahead of the duct.

Figure 14 shows the variation of normalized duct hammershock pressure ratio, $\Delta p_{duct}/(p_t)_\infty$, and duct Mach number before surge, M'_{duct}, with fuselage station calculated from the data of table 2. The unflagged circles designate $\Delta p_{duct}/(p_t)_\infty$ for the pressure ports on the duct inboard wall and the static-pressure port at the compressor face, which is also on the inboard side. The flagged circles show $\Delta p_{duct}/(p_t)_\infty$ for the duct outboard pressure port. The values of $\Delta p_{duct}/(p_t)_\infty$ for

the outboard port are lower than the values for the inboard ports, which shows that the hammershock strength is not uniform across the duct as the hammershock propagates upstream. This may result from duct curvature and an initially nonuniform shock front starting at the compressor face.

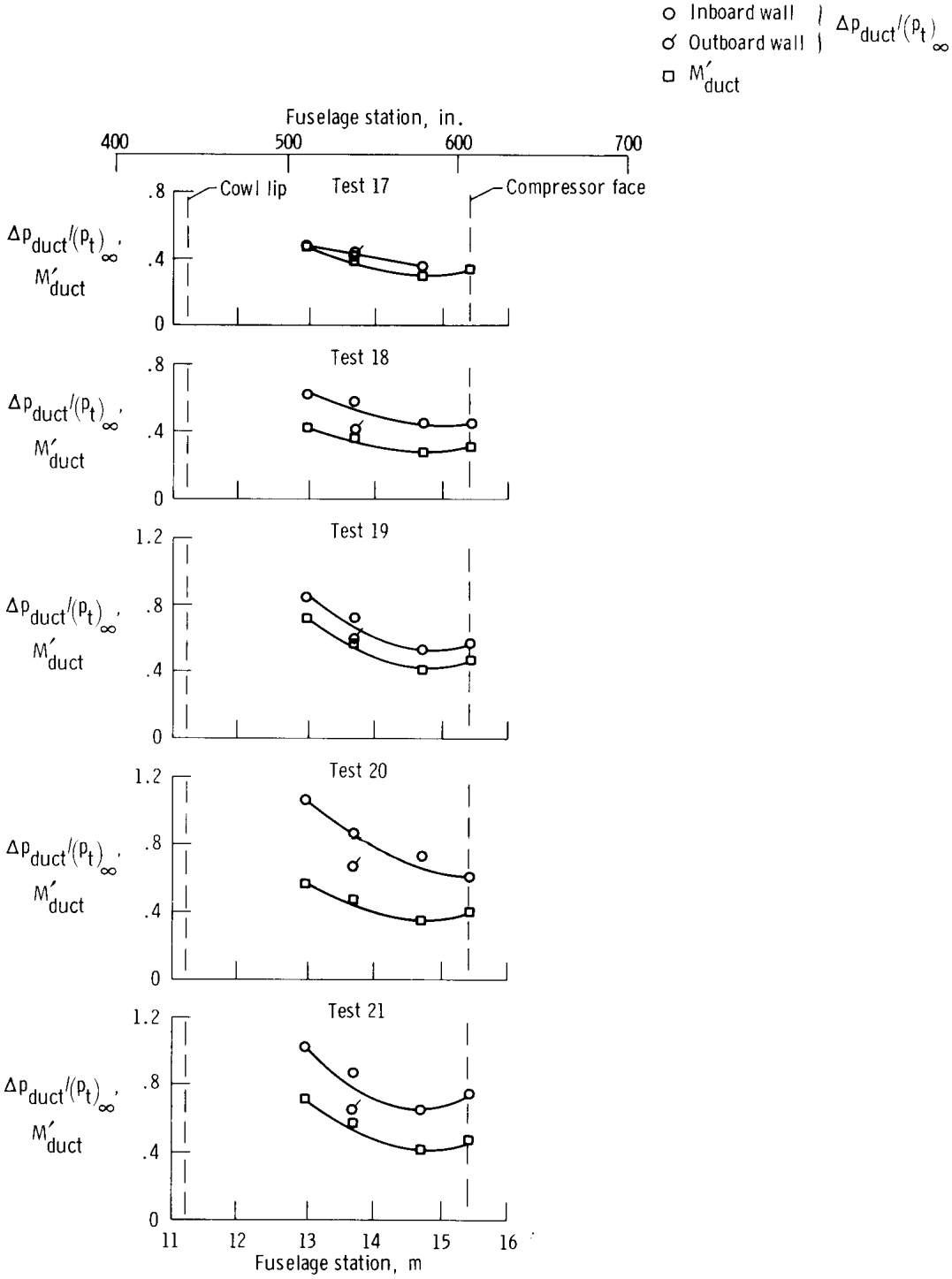

Figure 14. Variation of normalized duct hammershock pressure ratio and duct Mach number before surge along the duct.

The fairings of the M'_{duct} (squares) and $\Delta p_{duct}/(p_t)_\infty$ data in figure 14 are essentially parallel for most of the data, suggesting a relationship between these two variables. This relationship is indicated in figure 15, a plot of $\Delta p_{duct}/(p_t)_\infty$ against M'_{duct}, which shows linear trends for the duct inboard wall pressures. These data indicate that hammershock pressure ratio increases linearly with duct Mach number, which is in agreement with the results of the simplified theory discussed in the DATA ANALYSIS section. The data for the duct outboard wall do not conform to the linear trends.

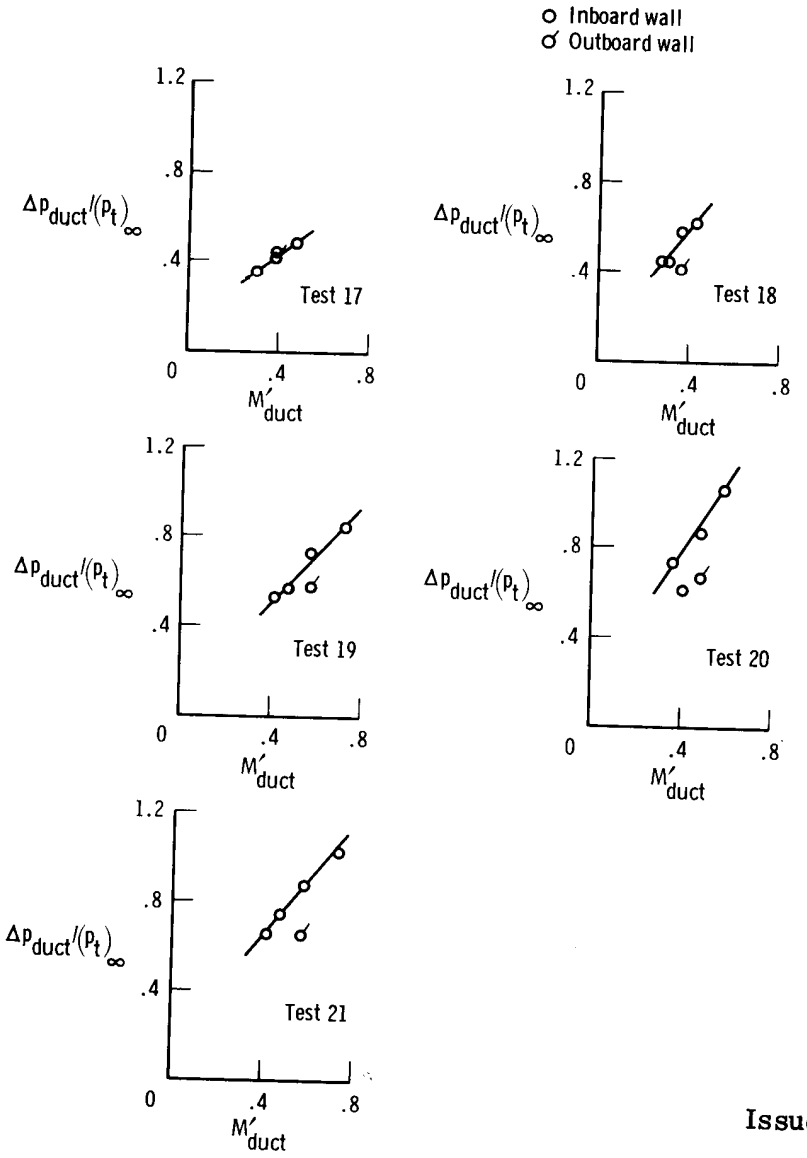

Issue date: 8-26-74

Figure 15. Effect of stabilized duct Mach number before surge on normalized duct hammershock pressures.

The transit time of the several hammershock pulses through the fixed-geometry portion of the duct in the number 6 airplane is shown in figure 16. The data show that transit time increased steadily with distance forward of the compressor face. Data scatter about the fairing was reasonably close to the sampling interval precision of 2.5 milliseconds. A theoretical transit time, assuming that the F-111A duct had a constant area, is also shown. The hammershock velocity of 274 meters per second (900 feet per second) was obtained from T_t = 320° K (570° R) and M_s = 0.77. These are typical values calculated from the data shown in table 2. The actual transit time agrees well with the theoretical transit time. A good approximation for the data shown is 3 milliseconds per meter (1 millisecond per foot) for transit time through the fixed-geometry portion of the duct.

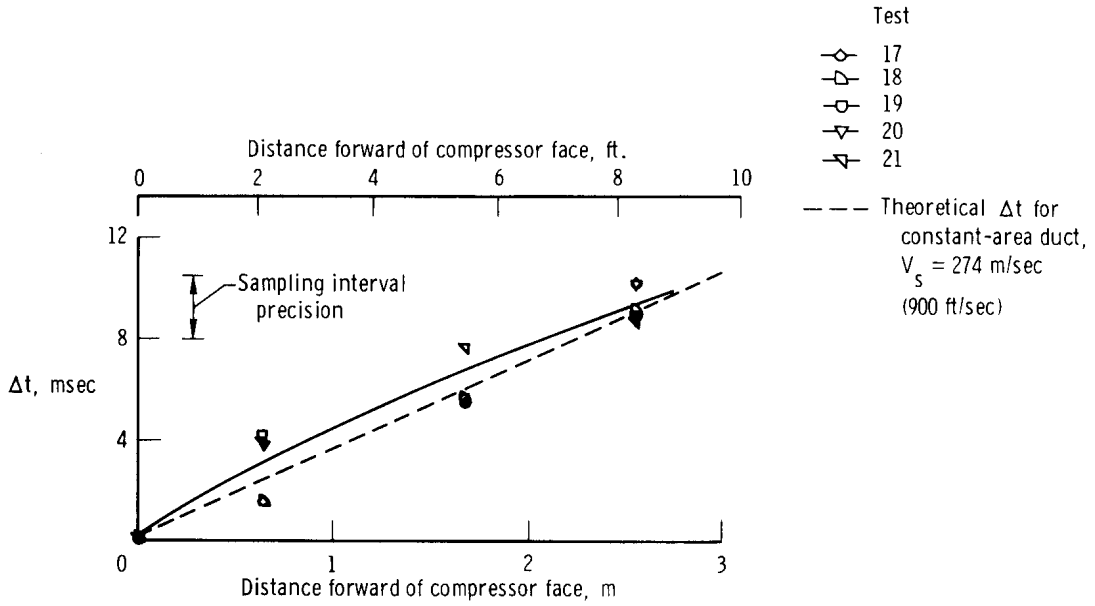

Figure 16. Transit time of hammershocks through fixed-geometry portion of duct on number 6 airplane.

CONCLUSIONS

Data from 21 flight tests involving compressor surges and hammershock transients on two F-111A airplanes were analyzed. The tests covered flight speeds from Mach 0.71 to Mach 2.23 and altitudes from approximately 3200 meters (10,600 feet) to 14,500 meters (47,500 feet). Hammershock data from a static ground run were also analyzed. The following conclusions were reached:

(1) Hammershock transients originating from engine compressor surges propagated forward through the duct and caused strong pressure rises at the compressor face and in the duct. These pressures were followed by a pressure decay when the high-pressure air in the duct was expelled through the cowl entrance. Hammershock transients sometimes induced additional transients, such as a rotating stall or duct buzz, before the engine recovered from the compressor surge.

(2) Hammershock pressure ratios at the compressor face were unaffected by free-stream Mach number or altitude, but were functions of compressor face Mach number and its related parameters, such as engine-corrected speed, engine-corrected airflow, and compressor pressure ratio. The maximum value of hammershock pressure ratio, approximately 1.83, occurred at a compressor pressure ratio of approximately 21.7.

(3) Hammershock pressure rise was proportional to core airflow preceding the surge. Hammershock pressure exceeded free-stream total pressure on all the tests; on two tests the difference approached 35 kN/m^2 (5 lbf/in^2).

(4) Normalized hammershock pressure ratio on the inboard wall of the duct increased linearly with duct Mach number preceding the compressor surge. Differences between hammershock pressures on the inboard and outboard walls indicated a nonuniform shock front. Hammershock transit time through the fixed-geometry portion of the duct was approximately 3 milliseconds per meter (1 millisecond per foot).

Flight Research Center
National Aeronautics and Space Administration
Edwards, Calif., Mar. 18, 1974

REFERENCES

1. Mays, Ronald A.: Inlet Dynamics and Compressor Surge. J. Aircraft, vol. 8, no. 4, Apr. 1971, pp. 219-226.

2. Dawson, C. R.: Simulation and Measurement of Pressure Transients in a Mixed-Compression Supersonic Intake During Engine Surge. AIAA Paper No. 71-671, 1971.

3. Morriss, D. P.; and Williams, D. D.: Free-Jet Testing of a Supersonic Engine/Intake Combination. Aeron. J. Roy. Aeron. Soc., vol. 74, Mar. 1970, pp. 212-218.

4. Alford, J. S.; and Victor, I. W.: Dynamic Measurements of Forward Gas Expulsion during High Speed Stall of Jet Engines. SAE paper 650840, 1965.

5. Hughes, Donald L.; Holzman, Jon K.; and Johnson, Harold J.: Flight-Determined Characteristics of an Air Intake System on an F-111A Airplane. NASA TN D-6679, 1972.

6. Martin, Richard A.; and Hughes, Donald L.: Comparisons of In-Flight F-111A Inlet Performance for On- and Off-Scheduled Inlet Geometry at Mach Numbers of 0.68 to 2.18. NASA TN D-6490, 1971.

7. Burcham, Frank W., Jr.; Hughes, Donald L.; and Holzman, Jon K.: Steady-State and Dynamic Pressure Phenomena in the Propulsion System of an F-111A Airplane. NASA TN D-7328, 1973.

8. Holzman, Jon K.; and Payne, Gordon A.: Design and Flight Testing of a Nullable Compressor Face Rake. NASA TN D-7162, 1973.

9. Mechtly, E. A.: The International System of Units - Physical Constants and Conversion Factors. Second Revision. NASA SP-7012, 1973.

10. Burcham, Frank W., Jr.; and Bellman, Donald R.: A Flight Investigation of Steady-State and Dynamic Pressure Phenomena in the Air Inlets of Supersonic Aircraft. Inlets and Nozzles for Aerospace Engines, AGARD CP-91-71, paper no. 24, Dec. 1971.

11. Sedgwick, T. A.; Brown, A. C.; and Stroud, J. F.: Correlation of Wind Tunnel and Flight Test Data on the Air Induction System of the F-104 Aircraft. WADC TR-59-176, Wright Air Dev. Center, U.S. Air Force, July 1959.

12. Rudinger, George: Wave Diagrams for Nonsteady Flow in Ducts. D. Van Nostrand Co., Inc., c.1955, p. 155.

13. Marshall, F. L.: Prediction of Inlet Duct Overpressures Resulting From Engine Surge. AIAA Paper No. 72-1142, 1972.

14. Braithwaite, Willis M.; and Vollmar, William R.: Performance and Stall Limits of a YTF30-P-1 Turbofan Engine With Uniform Inlet Flow. NASA TM X-1803, 1969.

TABLE 1.–PARAMETERS USED IN THE ANALYSIS OF COMPRESSOR FACE HAMMERSHOCK PRESSURES ON AIRPLANE NUMBER 12

Test	M_∞	h_p, m (ft)	$(P_t)_\infty$, kN/m² (lbf/in²)	$(T_t)_\infty$, °K (°R)	X/R	θ_c, deg	M'_2	$N_1/\sqrt{\theta}$, rpm	$\frac{w\sqrt{\theta}}{\delta}$, kg/sec (lbm/sec)	$(P'_t)_2$, kN/m² (lbf/in²)	p'_2, kN/m² (lbf/in²)	p'_4, kN/m² (lbf/in²)	p'_4/p'_2	Bypass ratio	w_{core}, kg/sec (lbm/sec)	$(P_t)_b$, kN/m² (lbf/in²)	$(P_t)_b/p'_2$	$(P_t)_b/p'_4$	$(P_t)_b - p'_2$, kN/m² (lbf/in²)
1	1.72	13,800 (45,300)	72.4 (10.5)	332 (599)	1.71	20.2	0.43	8,870	97.5 (215)	64.8 (9.4)	58.6 (8.5)	813 (118)	13.9	1.07	27.8 (61.2)	92.4 (13.4)	1.58	0.114	33.8 (4.9)
2	1.82	13,900 (45,700)	84.8 (12.3)	349 (629)	1.71	21.0	0.40	8,430	93.4 (206)	76.5 (11.1)	68.2 (9.9)	820 (119)	12.0	1.16	29.4 (64.8)	104.8 (15.2)	1.54	0.128	36.5 (5.3)
3	1.98	14,000 (45,900)	107.5 (15.6)	368 (663)	1.71	21.9	0.38	8,000	86.2 (190)	93.8 (13.6)	84.8 (12.3)	917 (133)	10.8	1.34	30.5 (67.2)	124.8 (18.1)	1.47	0.136	40.0 (5.8)
4	0.79	10,900 (35,600)	35.2 (5.1)	238 (429)	1.71	10.5	0.50	10,370	109.3 (241)	33.1 (4.8)	28.9 (4.2)	552 (80)	19.0	0.89	20.6 (45.5)	51.0 (7.4)	1.76	0.093	22.1 (3.2)
5	0.71	3,200 (10,600)	96.5 (14.0)	309 (556)	2.10	22.5	0.41	8,620	93.9 (207)	84.8 (12.3)	75.1 (10.9)	1,117 (162)	14.9	1.15	35.0 (77.2)	121.3 (17.6)	1.62	0.109	46.2 (6.7)
6	0.93	3,400 (11,100)	116.5 (16.9)	376 (676)	1.98	20.4	0.43	8,900	98.0 (216)	103.4 (15.0)	91.0 (13.2)	1,455 (211)	16.0	1.06	45.6 (100.5)	151.0 (21.9)	1.66	0.104	60.0 (8.7)
7	0	700 (2,300)	93.8 (13.6)	304 (548)	2.24	10.5	0.45	9,320	100.2 (221)	75.8 (11.0)	68.2 (9.9)	1,296 (188)	19.0	1.01	45.6 (100.5)	120.0 (17.4)	1.76	0.093	51.7 (7.5)
8	0.73	9,300 (30,500)	42.1 (6.1)	260 (469)	1.94	14.6	0.49	10,080	105.7 (233)	37.2 (5.4)	31.7 (4.6)	689 (100)	21.7	0.94	21.1 (46.5)	57.9 (8.4)	1.83	0.084	26.2 (3.8)
9	0.73	9,300 (30,500)	42.1 (6.1)	253 (456)	1.94	19.9	0.39	8,200	89.8 (198)	38.6 (5.6)	35.2 (5.1)	448 (65)	12.7	1.25	16.1 (35.5)	55.8 (8.1)	1.59	0.125	20.7 (3.0)
10	0.95	9,600 (31,400)	51.0 (7.4)	275 (495)	2.24	16.9	0.48	9,870	104.8 (231)	43.4 (6.3)	37.9 (5.5)	800 (116)	21.1	0.94	23.8 (52.5)	69.6 (10.1)	1.84	0.087	31.7 (4.6)
11	0.93	9,400 (30,800)	51.0 (7.4)	275 (495)	2.24	16.9	0.43	8,890	97.1 (214)	46.2 (6.7)	40.7 (5.9)	655 (95)	16.1	1.08	21.9 (48.3)	69.6 (10.1)	1.71	0.106	29.0 (4.2)
12	0.92	9,400 (30,800)	50.3 (7.3)	273 (492)	2.24	18.3	0.37	7,940	86.6 (191)	46.9 (6.8)	42.7 (6.2)	483 (70)	11.3	1.33	17.6 (38.8)	63.4 (9.2)	1.48	0.131	20.7 (3.0)
13	0.93	9,500 (31,000)	50.3 (7.3)	274 (494)	2.24	18.3	0.31	7,000	75.3 (166)	47.6 (6.9)	44.1 (6.4)	372 (54)	8.4	1.60	13.9 (30.7)	59.3 (8.6)	1.34	0.159	15.2 (2.2)
14	2.23	14,100 (46,400)	153.8 (22.3)	403 (726)	1.74	23.8	0.32	7,300	74.8 (165)	125.5 (18.2)	117.9 (17.1)	1,124 (163)	9.5	1.61	30.2 (66.6)	160.6 (23.3)	1.36	0.143	42.7 (6.2)
15	2.03	14,500 (47,500)	107.5 (15.6)	373 (671)	1.71	22.4	0.35	7,800	81.6 (180)	93.8 (13.6)	86.9 (12.6)	931 (135)	10.7	1.44	27.2 (60.0)	124.1 (18.0)	1.43	0.133	37.2 (5.4)
16	0.93	3,300 (10,900)	117.2 (17.0)	331 (595)	2.23	20.1	0.44	9,050	99.8 (220)	103.4 (15.0)	90.3 (13.1)	1,510 (219)	16.7	1.02	47.4 (104.5)	155.8 (22.6)	1.73	0.103	65.5 (9.5)

TABLE 2.—PARAMETERS USED IN THE ANALYSIS OF HAMMERSHOCK PROPAGATION ON AIRPLANE NUMBER 6

Test	M_∞	h_p, m (ft)	$(p_t)_\infty$, kN/m² (lbf/in²)	$(T_t)_\infty$, °K (°R)	X/R	θ_c, deg	A_c, m² (ft²)	M'_2	$N_1/\sqrt{\theta}$, rpm	$\frac{w\sqrt{\theta}}{\delta}$, kg/sec (lbm/sec)	$(p'_t)_2$, kN/m² (lbf/in²)	p'_2, kN/m² (lbf/in²)
17	1.97	13,100 (43,100)	121 (17.6)	389 (700)	1.80	19.8	0.435 (4.69) (a)	0.34	7,450	80.7 (178)	108 (15.6)	99.3 (14.4)
18	0.73	3,300 (10,900)	96.5 (14.0)	958 (532)	2.24	19.9	0.414 (4.45) (b)	0.31	6,930	74.4 (164)	92.4 (13.4)	86.2 (12.5)
19	0.73	9,390 (30,800)	41.4 (6.0)	814 (452)	2.24	18.5	0.423 (4.56) (b)	0.47	9,500	104 (229)	37.9 (5.5)	33.1 (4.8)
20	1.79	13,530 (44,400)	86.1 (12.5)	356 (640)	1.80	16.9	0.433 (4.66) (b)	0.40	9,170	105 (232)	77.2 (11.2)	69.6 (10.1)
21	0.94	9,500 (31,200)	50.3 (7.3)	266 (479)	2.24	16.9	0.414 (4.45) (b)	0.47	9,500	104 (229)	45.5 (6.6)	38.6 (5.6)

[a]Blunt-lip cowl.

[b]Sharp-lip cowl.

Test	M'_A	M'_B	M'_C	M'_D	$\frac{\Delta p_A}{(p_t)_\infty}$	$\frac{\Delta p_B}{(p_t)_\infty}$	$\frac{\Delta p_C}{(p_t)_\infty}$	$\frac{\Delta p_D}{(p_t)_\infty}$	$\frac{\Delta p_2}{(p_t)_\infty}$	$\frac{\Delta p_{cone}}{(p_t)_\infty}$
17	0.300	0.381	0.468	0.381	0.355	0.440	0.480	0.416	- - -	0.195
18	0.274	0.360	0.421	0.360	0.444	0.579	0.619	0.412	0.441	0.180
19	0.408	0.566	0.718	0.566	0.533	0.728	0.848	0.578	0.570	0.465
20	0.350	0.472	0.569	0.472	0.730	0.865	1.060	0.662	0.616	0.408
21	0.408	0.566	0.718	0.566	0.653	0.873	1.021	0.653	0.748	0.241